THE PUBLISHING HOUSE
OF THE ROMANIAN ACADEMY

PROCEEDINGS OF THE ROMANIAN ACADEMY, Series A,
Volume 20, Number 2/2019, pp. 141–150

OPTICAL ATTENUATORS WITH RISLEY PRISMS AND DISK CHOPPERS

Virgil-Florin DUMA[1,2]

[1] *Aurel Vlaicu* University of Arad, 3OM Optomechatronics Group, Arad 310130, Romania
[2] Polytechnic University of Timisoara, Doctoral School, Timisoara 300222, Romania
E-mail: duma.virgil@osamember.org

Abstract. We approach different types of optomechanical attenuators with shutters and filters. Common devices are reviewed, and their advantages and drawbacks are discussed from the point of view of a set of characteristic parameters – in contrast to other devices that we have developed and/or optimized. Polarizing and step-by-step filters are thus compared with the translational Risley prisms that we have developed; the optimal solution of the latter is presented. Commercially available shutters are pointed out, while choppers with disks are approached in detail for optical attenuation. For the latter, classical disks with windows with linear margins are considered, and their transmission coefficient is determined for finite diameter sections of top-hat laser beams in the plane of the disk. The case of beam sections with diameters smaller that the width of the chopper window is considered, as well as the case of beam sections that overlap the outer and/or inner window margins. The latter case is proposed as a solution to adjust the average transmission coefficient of the device.

Key words: optical attenuators, transmission coefficient, filters, shutters, Risley prisms, translational optical wedges, neutral density filters, optomechanics, disk choppers.

1. INTRODUCTION

Optical attenuators are utilized in numerous applications [1]. The most common devices are optomechanical, with different types of shutters and filters. Various such attenuators are commercially available, each of them with specific advantages and drawbacks that makes it more suitable for certain systems. Taking into account requirements of different applications, we have developed novel devices or optimized existing ones, often focusing on other functions than optical attenuation. Thus, we have utilized choppers [2-7] to generate controlled laser impulses [8-12]. We approached Risley prisms [13-15] as laser scanners [16], but also in their translational variant [17,18], as attenuators [19].

The aim of this work is to approach such devices as optical attenuators. Their characteristic functions and parameters are deduced in this respect, and compared with those of commercially available attenuators, including various types of shutters and filters. A classification of such devices in these two main types also define their two functioning principles [20]. Thus, shutters adjust the transmitted flux by modifying the dimension (of the section) of the light beam. In contrast, filters make this flux adjustment by modifying the intensity and/or the spectrum of the transmitted light beam (while its section remains essentially unchanged).

The remaining of this paper is structured as follows: Section 3 discusses optical filters, from classical polarizing and step-by-step filters to the optimization of the more fine tuning Risley prisms. Section 4 approaches shutters, from common iris diaphragms to disk choppers. Section 5 concludes the study and provides directions of future work.

2. GENERAL PARAMETERS OF OPTICAL ATTENUATORS

Regardless of the type of attenuator considered, the main function that characterizes such a device is

(i) *the transmission coefficient*:

$$\tau(x) = \Phi(x)/\Phi_i \ , \tag{1}$$

where x is the (generic, i.e. translational or rotational) adjustment parameter of the device, Φ_i is the incident (energetic/radiometric or photometric) light flux, and Φ is the emergent flux. Alternatively, one could use the attenuation coefficient 1-τ, as a black box model is considered throughout the study: all the light that is not transmitted is considered attenuated, regardless of the phenomenon involved, i.e. absorption, reflection on certain surfaces, polarization, chopping, etc.

The minimum and the maximum transmission levels of the device, τ_{min} and τ_{max} (involving a minimum and a maximum transmitted flux Φ_{min} and Φ_{max}, respectively) allow for defining [19]:

(ii) *the attenuation ratio*

$$k = \tau_{max} / \tau_{min} . \tag{2}$$

(iii) *the attenuation interval*

$$\Delta\tau = \tau_{max} - \tau_{min} . \tag{3}$$

In order to (still) provide a minimum (i.e., satisfactory) flux or illumination level in the optical system, (iv) *the minimum transmission coefficient* τ_{min} is also important. This is for example the situation in colorimetry, where not only k and $\Delta\tau$ are relevant (to provide an as large as possible distinguishable gamut of colors), as one cannot actually distinguish colors unless a minimum flux (therefore τ_{min}) is provided [21].

Finally, the finesse, as well as the linearity of the tuning of the transmitted flux has to be characterized, using: (v) *the sensitivity of the attenuator*

$$S(x) = d\tau / dx . \tag{4}$$

3. OPTICAL FILTERS AS ATTENUATORS

3.1. Polarizing and step-by-step filters

Numerous commercially available types of optical filters are utilized as attenuators. They can work in reflection or transmission (the latter with polarizing or absorption materials), they can be continuous or step-by-step, translational or rotational. A few of the most representative ones are pointed out in the following.

A pair of polarizing filters has (Fig. 1), from Malus' law, the transmission function

$$\tau(\varphi) = \frac{I_{An}}{I} = \frac{\tau_P^2}{2}\cos^2\varphi , \tag{5}$$

where φ is the angle between the axis of the polarizer (ΔPo) and of the analyzer (ΔAn); I is the intensity of the incident, natural light; I_{An} is the intensity of the light emerging the An; $\tau_P \approx 0.3$ is the common transmission coefficient of a filter.

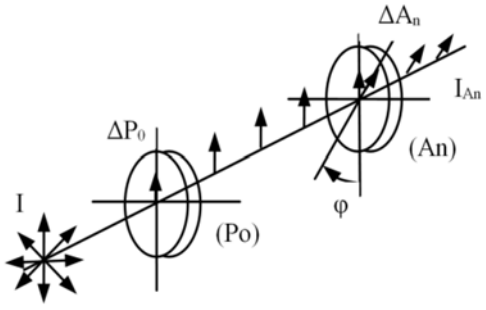

Fig. 1 – Optical attenuator with a pair of polarizing filters. Po, polarizer; An, analyzer.

While this attenuator has an interesting range from $\tau_{min}=0$ to $\tau_{max}=\tau_P^2/2$, it has the disadvantage of a non-linear transmission function, with $S(\varphi) \sim \sin 2\varphi$.

Transmission filters can perform a continuous adjustment, (with linear devices or rotational disks, Fig. 2a [22]) or a step-by-step attenuation. The former has a linear transmission characteristic – Fig. 2b, but the beam

has to be focused in the plane of the filter in order to perform such a transmission. The latter, more common in optical setups, can be done with rotational disks (with filters with thin films depositions) – Fig. 3a, with variable width plates – Fig. 3b, or, often, with sets of filters that can be utilized in various combinations.

The latter variant comprises the well-known pair of filter wheels where colored or neutral density filters can be mounted [22]. Commercially available (manual or motorized) double wheels (Thorlabs Inc, Newton, NJ, USA) for example have 6 or 24 filter mounts each, therefore such a device has $C_6^2 = 15$ or $C_{24}^2 = 276$ possible steps of the transmission coefficient, respectively. Micro-devices are also developed for fine tuning attenuation [23], but we focused on more sturdy, macro-devices, as presented in the following.

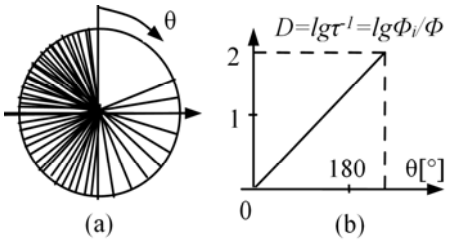

Fig. 2 – a) Circular attenuator with metallic film deposition; b) optical density D.

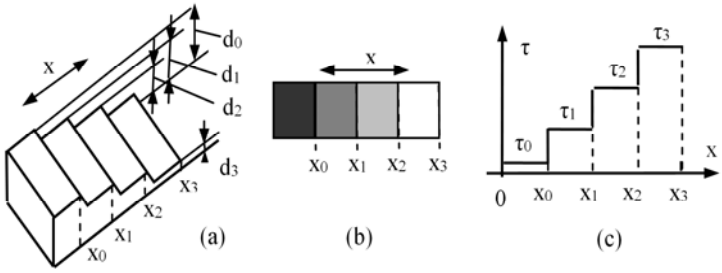

Fig. 3 – Step-by-step neutral density (ND) filters: a) with absorption filters; b) with metallic thin films; c) step-by-step transmission function.

3.2. Attenuators with translational Risley prisms

The issue of the above devices is the lack of controlled fine tuning of the transmission coefficient, Eq. (1). As we had to solve this for colorimetry applications, we have approached a different type of attenuator, with a pair of translational Risley prisms [19]. As in the literature two such devices were mentioned (but without characteristic parameters), we investigated all their three possible variants: (i) with a fix prism and a mobile one sliding along the hypotenuse; (ii) with both prisms moving symmetrically in opposite directions; (iii) with a fix prism and a mobile one sliding parallel to a leg. We demonstrated that the second variant is the best both from a mechanical and an optical point of view [19], and also developed its designing calculus.

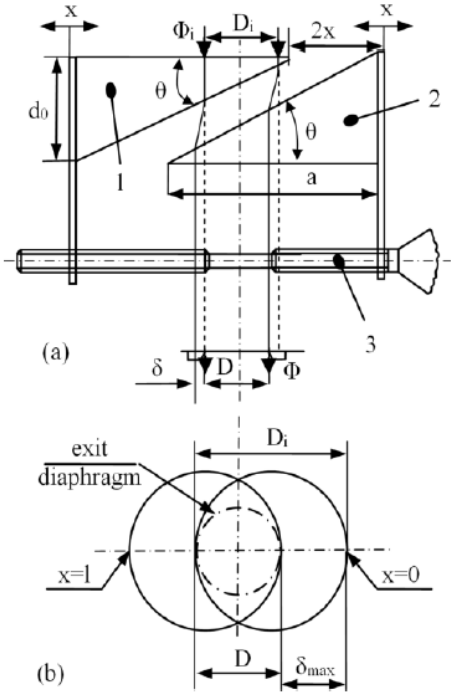

Fig. 4 – Optical attenuator with symmetrically moving translational Risley prisms, developed in detail in [19]. Not at scale.

For the device in Fig. 4, using Lambert-Beer's law, the flux Φ_e that emerges the two identical prisms is:

$$\Phi_e(x) = \Phi_i \cdot \exp\left(-\alpha \cdot d(x)\right), \tag{6}$$

where α is the absorption coefficient, while the current thickness of the filter formed by the prisms can be deduced as (Fig. 4)

$$d(x) = d_0 - (2x + \delta)\tan\theta. \tag{7}$$

In this expression θ is the prism angle, $x = 0\ldots\ x_{\max}$ is the (equal, but in opposite directions) displacement of each prism, d_0 is the maximum possible width of the plate that can be formed, and δ is the displacement of the light beam passing through the prisms:

$$\delta(x) = 2x \cdot \left[n\cos\theta \Big/ \sqrt{1 - n^2\sin^2\theta} - 1 \right] \sin^2\theta, \tag{8}$$

where n is the refractive index of the prisms. In order to maintain unchanged the exit diameter D (e.g., in colorimetry), a diaphragm is placed at the exit of the prism assembly – Fig. 4. Taking this into account and by imposing the condition to use the full length $a = D + 2x_{\max} + \delta_{\max}$ of a prism, from Eqs. (6) and (7) the transmission function of the device, Eq. (1), is (Fig. 5):

$$\tau(x) = r_1\tau_0 \exp[2r_2 \cdot \alpha \cdot x \cdot \tan\theta], \tag{9}$$

where $\tau_0 = \exp(\alpha \cdot d_0)$ and two coefficients were introduced [19]:

$$r_1 = \left(D / D_i\right)^2; \quad r_2 = \left(n\sin^2\theta \Big/ \sqrt{1 - n^2\sin^2\theta} + \cos\theta \right)\cos\theta. \tag{10}$$

$\delta_{\max} = \delta(x = x_{\max})$ is the maximum displacement of the beam.

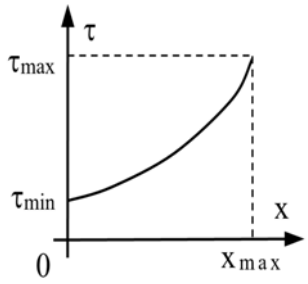

Fig. 5 – Transmission curve of a Risley prisms attenuator [19].

The extreme values of the transmission coefficient are obtained, using Eq. (9), for $x = 0$ and $x = x_{\max}$ (Fig. 5):

$$\tau_{\min} = r_1\tau_0 \quad \text{and} \quad \tau_{\max} = r_1\tau_0^{1-r_2}C^{r_2}, \tag{11}$$

respectively, where the $C = \exp(-\alpha \cdot D_i \cdot \tan\theta)$ constant was introduced.

Using Eqs. (11), from Eqs. (2) and (3), the characteristic parameters of the attenuator, i.e. its transmission ratio and interval are [19]:

$$k = \left(C/\tau_0\right)^{r_2} \quad \text{and} \quad \Delta\tau = r_1\tau_0\left[\left(C/\tau_0\right)^{r_2} - 1\right], \tag{12}$$

and from Eq. (4), the sensitivity of the device is

$$S(x) = 2r_2 \cdot \alpha \cdot \tau(x) \cdot \tan\theta. \tag{13}$$

The non-linearity of the characteristic function (reflected in this non-constant sensitivity) is one of the issues of this attenuator. The other one is the limited attenuation range, of approximately 2.5× demonstrated in [19] for the optimal prism angle, $\theta \approx 10^o$. The advantages of this solution are its small error regarding the

transmission coefficient (evaluated in [19] to a maximum of 0.002% because of high-precision available components), but more important its fine tuning. The latter is the one that makes the device appropriate for colorimetry: it allows for a fine adjustment of color coordinates by finely tuning the flux of color components in a mixture [21].

4. SHUTTERS AS OPTICAL ATTENUATORS

4.1. Classical shutters

Translational shutters are the most well-known, because of their early and extensive use in photographic cameras. It is worth mentioning that their simple principle (which is not discussed here) also stands for the functioning of novel devices that, to our knowledge, we have introduced, i.e., choppers with rotational shafts that are capable to reach much higher chop frequencies than disk choppers [11].

Another attenuator is the iris diaphragm, common as a macro-, but also developed as a micro-device [24]. Its transmission coefficient is (Fig. 6)

$$\tau(\varphi) = \Phi(\varphi)/\Phi_i = \left(D(\varphi)/D_i\right)^2, \tag{14}$$

where D_i is the diameter of the incident beam and $D = D_{\min} \ldots D_{\max}$ is the diameter of the emergent beam; the latter is a function of the (manually or motorized [22]) rotational (adjusting) angle φ of the precision screw.

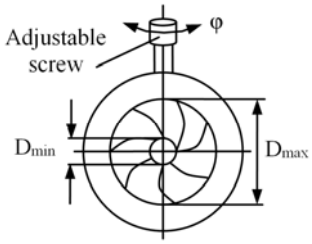

Fig. 6 – Iris diaphragm.

4.2. Optical attenuators with disk choppers

Such types of shutters are more complex and interesting. A chopper with a rotational disk in its classical configuration (i.e., with windows with linear margins) is presented in Fig. 7a. While in practice it is common to consider the light (usually laser) beam perfectly focused in the plane of the disk, this ideal situation is actually not met. Thus, in a rigorous approach one must take into account the finite diameter $2r$ of the beam section in the plane of the disk – Fig. 7a [8]. This means that the laser pulses produced by the device (when chopping the incident continuous wave laser beam) do not have an ideal, rectangular shape, but a shape like the one in Fig. 7b, with transition periods of time intervals $\tau = 2\delta/\omega$, where 2δ is the angle the beam section is seen from the pivot O of the disk, and ω is the rotational speed of the disk – Fig. 7a.

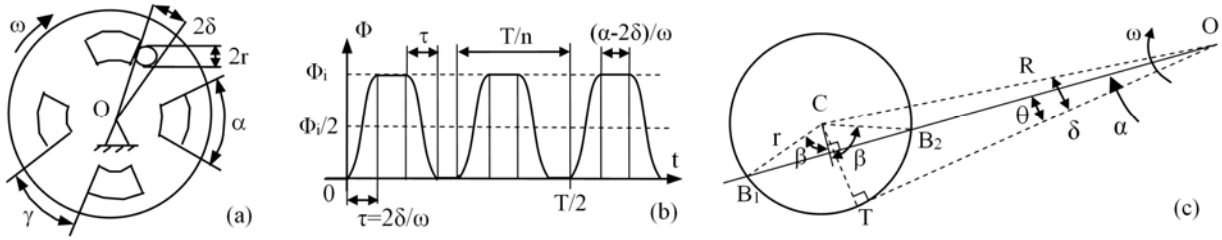

Fig. 7 – a) Chopper with disk with windows with linear margins (at $t = 0$, when the window margin is tangent to the beam section); b) transmission function (top-hat laser pulses); c) un-obscuration of the beam section in the plane of the disk.

The time intervals τ characterize both the obscuration and the un-obscuration periods – Fig. 7c, while the period of full transmission has the time interval $(\alpha-2\delta)/\omega$, where α is the angle of a window – Fig. 7a. The angle of a wing is $\gamma = 2\pi/n - \alpha$, where n is the number of windows of the disk.

In order to characterize the light transmission through the chopper, in Fig. 7a the $t=0$ moment is considered when the margin of a window is tangent to the section of the beam, in the point T – Fig. 7c, and the un-obscuration of the beam begins. For a top-hat laser beam (i.e., with a constant intensity on the entire beam section), the light flux transmitted is:

$$\Phi(\theta) = \Phi_i \frac{S(\theta)}{\pi r^2}, \tag{15}$$

where $\theta = \omega \cdot t$, as $\omega = cst.$ and $S(\theta)$ is the uncovered area of the beam section. Using Fig. 7c,

$$B_1B_2 = 2\,CS \cdot \mathrm{tg}\beta, \quad CS = r\cos\beta = R\,\sin(\delta-\theta). \tag{16}$$

The semi-angle that characterizes the position of the chopper blade (its intersection points B_1 and B_2 with the beam section) is therefore, from Eq. $(16)_2$,

$$\beta(\theta) = \arccos\frac{\sin(\delta-\theta)}{\sin\delta}, \tag{17}$$

where $\sin\delta = r/R$. From Eqs. (15) to (17),

$$S\big(\beta(\theta)\big) = \beta r^2 - \frac{CS \cdot B_1B_2}{2} = r^2\left(\beta - \frac{\sin 2\beta}{2}\right). \tag{18}$$

From Eqs. (1), (15), and (18), the transmission function for the un-obscuration of the beam section is:

$$\tau(\theta) = \frac{1}{\pi}\left(\beta - \frac{\sin 2\beta}{2}\right) = \frac{1}{\pi}\left(\arccos\frac{\sin(\delta-\theta)}{\sin\delta} - \frac{\sqrt{\sin\theta\cos(2\delta-\theta)}}{\sin^2\delta}\sin(\delta-\theta)\right), \text{ for } \theta\in[0,2\delta]. \tag{19}$$

In a similar way, for the obscuration of the beam section – Fig. 7, the transmission function is:

$$\tau'(\theta) = 1 - \frac{1}{\pi}\left(\arccos\frac{\sin(\delta-\theta+\alpha)}{\sin\delta} - \frac{\sqrt{\sin(\theta-\alpha)\cos(2\delta-\theta+\alpha)}}{\sin^2\delta}\sin(\delta-\theta+\alpha)\right), \text{ for } \theta\in[\alpha,\alpha+2\delta]. \tag{20}$$

The graphs of the functions $\Phi(\theta)$ and $\Phi'(\theta)$, proportional to the coefficients $\tau(\theta)$ and $\tau'(\theta)$, respectively, are shown in Fig. 8.

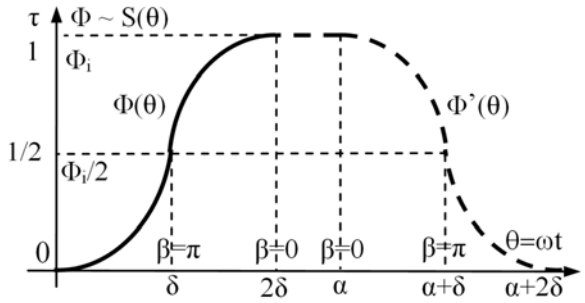

Fig. 8 – The area of the beam section that is uncovered by the chopper window.

In order to determine the parameter of interest in this case, i.e., **the average/total transmission coefficient** (on a rotation period $T=2\pi/\omega$), one has to study the symmetry of these functions. One can see that the two graphs in Fig. 8 are not symmetrical with regard to their middle vertical line (i.e., from Eq. (19): $\Phi(\theta) + \Phi(2\delta-\theta) \neq \Phi_i$, and from Eq. (20): $\Phi'(\theta)+\Phi'(2\alpha+2\delta-\theta) \neq \Phi_i$), but from these equations

$$\Phi(\theta) + \Phi'(\alpha+\theta) = \Phi_i. \tag{21}$$

In consequence, the average transmission coefficient (considered for a sufficiently large time interval, for example for a number of rotation periods T) is from Fig. 7b, using Talbot's law,

$$\tau_{\text{total}} = \frac{\Phi_i\left(\alpha - 2\delta + 4\delta/2\right)/\omega}{\Phi_i 2\pi/n\omega} \quad \Rightarrow \quad \tau_{\text{total}} = \frac{\alpha}{2\pi/n}. \tag{22}$$

It is interesting that in the ideal situation of a beam perfectly focused in the plane of the chopper disk, for which the transmission function in Fig. 7b would consist of rectangular impulses, this coefficient is

$$\tau_{\text{total}} = \frac{\Phi_i \alpha/\omega}{\Phi_i 2\pi/n\omega} \quad \Rightarrow \quad \tau_{\text{total}} = \frac{\alpha}{2\pi/n}. \tag{23}$$

In conclusion **the average/total transmission coefficient is an invariant of this device with regard to the size of the beam section**.

It is worth mentioning in this respect that the chopper solutions patented in [12] approached the adjustment of this average coefficient, by proposing a device with two identical disks superposed to each other, which allows for fixing a certain angle α of each window before starting the chopper.

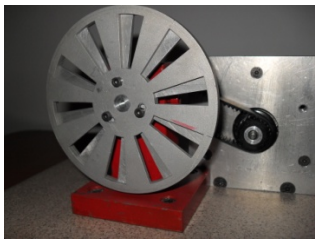

Fig. 9 – Double disk chopper [12], with the technology developed in [10].

4.3. Disk choppers with eccentric beam sections

Another possibility to adjust the coefficient τ_{total}, different than the one in Fig. 9 is to use a laser beam section eccentric with regard to the upper and/or to the lower margins of the window (i.e., overlapping them), as shown in Fig. 10a: tangent to (i) the lower or to (ii) the upper limit; (iii) with outer margins, centered on the middle circle of the window. These particular cases are considered in order to be able to assure these positions in a precise way in optical setups.

The lower and the upper margins of the window are characterized by the radius R_1 and R_2, respectively. Therefore the radius of the middle circle of the window and the window semi-width are respectively

$$R = (R_1 + R_2)/2 \quad \text{and} \quad \rho = (R_2 - R_1)/2. \tag{24}$$

The three cases in Fig. 10a therefore correspond to $r > \rho$ and: (i) $\text{OC} - r = R_1$; (ii) $\text{OC} + r = R_2$; (iii) $\text{OC} = R$, where OC is the distance between the pivot O of the disk and the center C of the beam section.

The ascertainment of the transmitted flux for cases (i) and (ii) is made in Figs. 10b and 10c, respectively.

The transmitted flux for top-hat laser beams is, as in the previous subsection, proportional to the uncovered area of the beam section in the plane of the chopper. The problem is to determine the maximum achievable transmitted flux, which is proportional to the maximum area that can be uncovered from the beam section: for case (i), $\pi r^2 - A(\text{MPNQ})$, Fig. 10b; for case (ii), $\pi r^2 - A(\text{M}'\text{P}'\text{N}'\text{Q}'')$, Fig. 10c.

Case i. From the geometry in Fig. 10b

$$\cos\varepsilon = \left[\text{OC}^2 + R_2^2 - r^2\right] \Big/ \left[2 \cdot \text{OC} \cdot R_2\right]; \tag{25}$$

$$\text{DN} = r\sin\angle\text{PCN} = R_2 \sin\varepsilon; \quad \text{OD} = R_2\cos\varepsilon; \quad \text{CD} = r\cos\angle\text{PCN}. \tag{26}$$

Taking these relationships into account, one can obtain the area outside the uncovered beam section:

$$A\left(\text{MPNQ}\right) = A\left(\text{MPND}\right) - A\left(\text{MQND}\right), \tag{27}$$

where, using Eqs. (26),

$$A(\mathrm{MPND}) = \mathrm{M\overset{\frown}{P}N}\cdot r/2 - \mathrm{DN}\cdot\mathrm{CD} = r^2\left(\measuredangle \mathrm{PC}N - \sin\measuredangle\mathrm{PCN}\cdot\cos\measuredangle\mathrm{PCN}\right) \tag{28}$$

$$A(\mathrm{MQND}) = A(\mathrm{MONQ}) - A(\mathrm{MON}) = \varepsilon\cdot R_2^2 - \mathrm{DN}\cdot\mathrm{OD} = R_2^2\left(\varepsilon - \sin\varepsilon\cdot\cos\varepsilon\right). \tag{29}$$

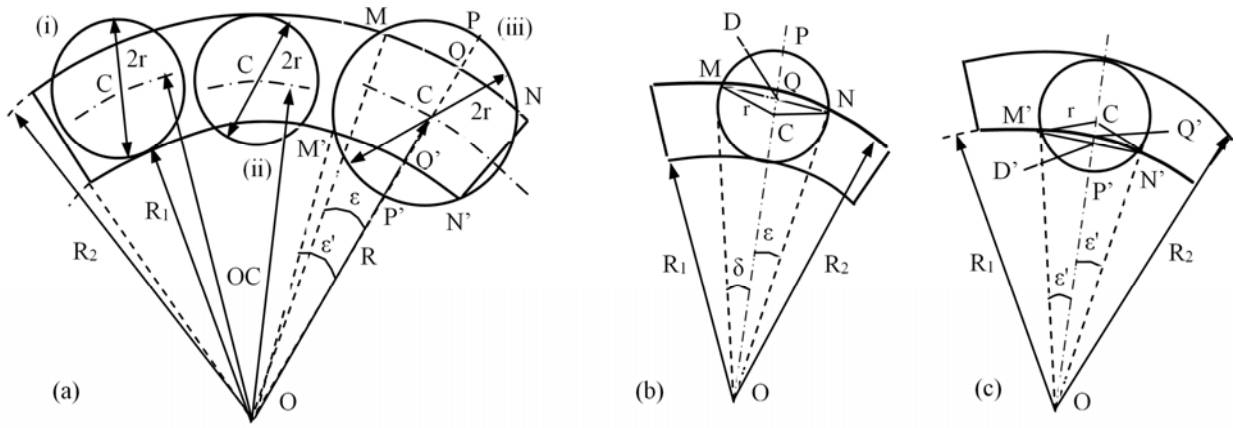

Fig. 10 – a) Disk chopper – different overlapping positions of the laser beam section with regard to the upper and lower margins of the window: tangent to (i) the inner margin or to (ii) the upper margin; (iii) section overlapping both margins centered on the middle circle of the window; b) and c) ascertainment of the transmitted flux for case (i) and (ii), respectively.

Therefore, from Eq. (27), with (28) and (29),

$$A(\mathrm{MQNP}) = r^2\left(\arcsin\frac{R_2\sin\varepsilon}{r} - \frac{R_2\sin\varepsilon}{r}\sqrt{1-\frac{R_2^2\sin^2\varepsilon}{r^2}}\right) - R_2^2\left(\varepsilon - \frac{\sin 2\varepsilon}{2}\right), \tag{30}$$

where for the particular case of the beam section tangent to the inner margin of the window, $\mathrm{OC}=R_1+r$, thus

$$\cos\varepsilon = \left[R^2+\rho^2+r(R-\rho)\right]\Big/\left[R^2-\rho^2+r(R+\rho)\right]. \tag{31}$$

Case ii. From the geometry in Fig. 10c the angle

$$\cos\varepsilon = \left[\mathrm{OC}^2 + R_1^2 - r^2\right]\Big/\left[2\cdot\mathrm{OC}\cdot R_1\right]; \tag{32}$$

$$\mathrm{D'N'} = r\sin\measuredangle\mathrm{P'CN'} = R_1\sin\varepsilon';\quad \mathrm{OD'} = R_1\cos\varepsilon';\quad \mathrm{CD'} = r\cos\measuredangle\mathrm{P'CN'}. \tag{33}$$

Taking these relationships into account, one can obtain the area outside the uncovered beam section:

$$A(\mathrm{M'P'N'Q'}) = A(\mathrm{M'P'N'D'}) - A(\mathrm{M'Q'N'D'}), \tag{34}$$

where, using Eqs. (33),

$$A(\mathrm{M'P'N'D'}) = A(\mathrm{M'CN'P'}) - A(\mathrm{M'CN'}) = r^2\left(\measuredangle\mathrm{P'CN'} - \sin\measuredangle\mathrm{P'CN'}\cdot\cos\measuredangle\mathrm{P'CN'}\right) \tag{35}$$

$$A(\mathrm{M'Q'N'D'}) = A(\mathrm{M'ON'Q'}) - A(\mathrm{M'ON'}) = \varepsilon'\cdot R_1^2 - \mathrm{D'N'}\cdot\mathrm{OD'} = R_1^2\left(\varepsilon' - \sin\varepsilon'\cdot\cos\varepsilon'\right) \tag{36}$$

Therefore, from Eq. (34), with (35) and (36),

$$A(\mathrm{M'Q'N'P'}) = r^2\left(\arcsin\frac{R_1\sin\varepsilon'}{r} - \frac{R_1\sin\varepsilon'}{r}\sqrt{1-\frac{R_1^2\sin^2\varepsilon'}{r^2}}\right) - R_1^2\left(\varepsilon' - \frac{\sin 2\varepsilon'}{2}\right), \tag{37}$$

where for the particular case of the beam section tangent to the inner margin of the window, $\mathrm{OC}=R_2-r$, thus

$$\cos\varepsilon' = \left[R^2 + \rho^2 - r(R+\rho)\right] \Big/ \left[R^2 - \rho^2 - r(R-\rho)\right]. \tag{38}$$

Case iii: From Fig. 10(a) the maximum area that can be uncovered is, with Eqs. (30) and (37),

$$A(\mathrm{MM'N'N}) = \pi r^2 - A(\mathrm{MQNP}) - A(\mathrm{M'Q'N'P'}). \tag{39}$$

5. DISCUSSION AND CONCLUSIONS

An overview of some of the most common optical attenuators was made, while two devices were approached in detail: with **translational Risley prisms** [19] and with **classical disks choppers** [8-12]. The former provides a fine tuning of the transmission, while the later has an average coefficient. However, choppers have the advantage of being able to selectively obscure certain wavelengths by adjusting the chopper frequency. A synoptic view of some of the attenuators characteristics is provided in Table 1.

Table 1

Characteristics of several types of optical attenuators with filters or shutters

Device	Parameter	$\tau(x)$	k	$\Delta\tau$	τ_{min}	S	*Remarks*
Filter	Pair of polarizing filters (Fig. 1)	non-lin.	-	$\tau_P^2/2$	0	not cst.	Continuous tuning
	Rotational disk filters (Fig. 2)	$\lg\tau = \mathrm{cst}$	Depends on the variant			cst.	Beam must be focused
	Variable width filter (Fig. 3) Step-by-step thin film filters [22]	Step-by-step	Depends on the variant		τ_0	cst. on steps	Translational. Less used
	Double filter disks (m windows)	C_m^2 steps	Depends on the filters used; $\tau_{max} = 0$			cst. on steps	Most used; practical; usually sufficient steps
	Risley prisms (Fig. 4) [19]	non-lin.	Eqs. (12) and (11)			not cst.	Fine tuning of $\tau(x)$
Shutter	Translational [22]	non-lin.	-	τ_{max}	0	not cst.	-
	Iris diaphragm (Fig. 6)	non-lin.	From Eq. (14)			not cst.	Tunes radius or flux
	Classical chopper (Figs. 7-10)	Produces various laser pulses. τ_{total} – Eq. (22) or (39)					
	Eclipse chopper [9, 12]	Produces approximately triangular laser pulses. τ_{total} – from [9]					
	Chopper with shaft [11]	Similar to translational, but the beam is obscured from both sides					

For choppers, top-hat laser beams have been considered, both with sections placed entirely inside the chopper's window and with sections that overlap the upper and/or inner margins of the window. The latter is an alternative to the chopper windows with adjustable angles, which is one of the claims in [12]. Future work includes Gaussian or Bessel beams to generate laser impulses, both with classical chopper disks and with the eclipse choppers that we have proposed [9] and patented [12]. A particularly interesting direction of work comprises the development and study of the much faster choppers with shafts that, to our knowledge, we have introduced – patent pending [11, 25].

ACKNOWLEDGEMENTS

This research was supported by the Romanian National Authority for Scientific Research through CNDI–UEFISCDI Grant PN-III-P2-2.1-BG-2016-0297 (http://3om-group-optomechatronics.ro/).

REFERENCES

1. M. BASS, Ed., *Handbook of Optics*, 3rd Edition, Mc. Graw-Hill Inc., New York, 2009, pp. 30.1–30.68.
2. K. BENJAMIN, A. ARMITAGE, R. SOUTH, *Harmonic errors associated with the use of choppers in optical experiments*, Measurement, **39**, *8*, pp. 764–770, 2006.
3. R.M. MATCHKO, G.R. GERHART, *High-speed imaging chopper polarimetry*, Opt. Eng., **47**, *1*, 016001, 2008.
4. D. GIRALDO, H. CORREA, D. PEÑA LARA, *Implementation of a programmable electromechanical chopper with adjustable frequency and duty cycle for specific heat measurements*, Measurement, **110**, pp. 60–64, 2017.

5. S. SONG, G. LI, X. HOU, S. ZHANG, Y. YU, L. LIN, *Principal frequency component analysis based on modulate chopper technique used in diffuse reflectance spectroscopy measurement*, Appl. Opt., **57**, *5*, pp. 1043–1049, 2018.
6. M. T. CHING, R. A. BRENNEN, R. M. WHITE, *Microfabricated optical chopper*, Opt. Eng., **33**, *11*, pp. 3634–3642, 1994.
7. M. UEDA, T. SHIONO, T. ITO, K. YOKOYAMA, *High-efficiency diffractive micromachined chopper for infrared wavelength and its application to a pyroelectric infrared sensor*, Appl. Opt., **37**, *7*, pp. 1165–1170, 1998.
8. V.-F. DUMA, *Theoretical approach on optical choppers for top-hat light beam distributions*, J. of Optics, **10**, *6*, 064008, 2008.
9. V.-F. DUMA, *Optical choppers with circular-shaped windows: Modulation functions*, Communications in Nonlinear Science and Numerical Simulation, **16**, *5*, pp. 2218–2224, 2011.
10. V.-F. DUMA, *Prototypes and modulation functions of classical and novel configurations of optical chopper wheels*, Latin American Journal of Solids and Structures, **10**, *1*, pp. 5–18, 2013.
11. V.-F. DUMA, D. DEMIAN, *Optical modulator, has solid rotating shaft with some through slots of well-defined profiles*, Romanian Patent No. RO129610-A0, 2014.
12. V.-F. DUMA, M. F. NICOLOV, C. MNERIE, L. SZANTHO, *Optical modulator with rotating element, has role to generate light pulses of certain profile*, Romanian Patent RO 126505, 2016.
13. Y. LI, *Third-order theory of the Risley-prism-based beam steering system*, Appl. Opt., **50**, *5*, pp. 679–686, 2011.
14. Y. ZHOU, D. FAN, S. FAN, Y. CHEN, G. LIU, *Laser scanning by rotating polarization gratings*, Appl. Opt., **55**, *19*, pp. 5149–5157, 2016.
15. A. LI, W. Yi, Q. ZUO, W. SUN, *Performance characterization of scanning beam steered by tilting double prisms*, Opt. Express, **24**, *20*, pp. 23543–23556, 2016.
16. V.-F. DUMA, A. SCHITEA, *Laser scanners with rotational Risley prisms: Exact scan patterns*, Proceedings of the Romanian Academy, Series A, **19**, *1*, pp. 53–60, 2018.
17. G. GARCIA-TORALES, M. STROJNIK, G. PAEZ, *Risley prisms to control wave-front tilt and displacement in a vectorial shearing interferometer*, Appl. Opt., **41**, *7*, pp. 1380–1384, 2002.
18. K. OKA, T. KANEKO, *Compact complete imaging polarimeter using birefringent wedge prisms*, Opt. Express, **11**, *13*, pp. 1510–1519, 2003.
19. V.-F. DUMA, M. NICOLOV, *Neutral density filters with Risley prisms: analysis and design*, Appl. Opt., **48**, *14*, pp. 2678–2685, 2009.
20. V.-F. DUMA, M. NICOLOV, M. KISS, *Optical choppers: modulators and attenuators*, Proc. SPIE, **7469**, 74690V, 2010.
21. G. WYSZECKI, W. S. STILES, *Color Science: concepts and methods, quantitative data and formulae*, Willey & Sons, 2000.
22. https://www.thorlabs.com/ (accessed on September 29, 2018).
23. X. WANG, H. REN, *Dielectrically actuated attenuator at 1.55 μm*, J. of Physics Comm., **22**, *8*, 085026, 2018.
24. R. R. A. SYMS, H. ZOU, J. STAGG, H. VELADI, *Sliding-blade MEMS iris and variable optical attenuator*, J. Micromech. Microeng., **14**, *12*, p. 1700, 2004.
25. V.-F. DUMA, D. DEMIAN, E. S. CSUKAS, N. POP, O. CIRA, *Non-conventional optomechanical choppers: analysis and design of novel prototypes*, Proc. SPIE, **10448**, 104481W, 2017**.**

Received October 13, 2018